Journal of the Mechanics and Physics of Solids 112 (2018) 458–471

Contents lists available at ScienceDirect

Journal of the Mechanics and Physics of Solids

journal homepage: www.elsevier.com/locate/jmps

Puncture mechanics of soft elastomeric membrane with large deformation by rigid cylindrical indenter

Junjie Liu[a], Zhe Chen[a], Xueya Liang[a], Xiaoqiang Huang[a], Guoyong Mao[a], Wei Hong[a,b], Honghui Yu[c], Shaoxing Qu[a,*]

[a] State Key Laboratory of Fluid Power & Mechatronic System, Key Laboratory of Soft Machines and Smart Devices of Zhejiang Province, and Department of Engineering Mechanics, Zhejiang University, Hangzhou 310027, China
[b] Department of Aerospace Engineering, Iowa State University, Ames, IA 50010, USA and Global Station for Soft Matter, Global Institution for Collaborative Research and Education, Hokkaido University, Sapporo 060-0810, Japan
[c] Department of Mechanical Engineering, The City College of New York, New York, NY 10031, USA

ARTICLE INFO

Article history:
Received 12 November 2017
Revised 24 December 2017
Accepted 6 January 2018
Available online 8 January 2018

Keywords:
Friction
Soft elastomeric membrane
Indentation
Puncture
Large deformation

ABSTRACT

Soft elastomeric membrane structures are widely used and commonly found in engineering and biological applications. Puncture is one of the primary failure modes of soft elastomeric membrane at large deformation when indented by rigid objects. In order to investigate the puncture failure mechanism of soft elastomeric membrane with large deformation, we study the deformation and puncture failure of silicone rubber membrane that results from the continuous axisymmetric indentation by cylindrical steel indenters experimentally and analytically. In the experiment, effects of indenter size and the friction between the indenter and the membrane on the deformation and puncture failure of the membrane are investigated. In the analytical study, a model within the framework of nonlinear field theory is developed to describe the large local deformation around the punctured area, as well as to predict the puncture failure of the membrane. The deformed membrane is divided into three parts and the friction contact between the membrane and indenter is modeled by Coulomb friction law. The first invariant of the right Cauchy-Green deformation tensor I_1 is adopted to predict the puncture failure of the membrane. The experimental and analytical results agree well. This work provides a guideline in designing reliable soft devices featured with membrane structures, which are present in a wide variety of applications.

1. Introduction

Soft elastomeric membrane structures are widely used and commonly found in engineering and biological applications, such as architecture membrane structure, the chamber wall of pneumatic soft robotic, and diaphragm in living body (Martinez et al., 2013; Parthasarathy and Groves, 2006; Mao et al., 2015). Compared with the hard solid structures, they feature the ability of spanning relatively large areas with small volume or weight (Pamplona et al., 2014; Pearce et al., 2011). Indentation of soft elastomeric membrane by rigid objects with different profiles is a common way to induce large local strain in the membrane (Begley et al., 2004; Scott et al., 2004; Selvadurai, 2006; Selvadurai and Yu, 2006; Yang and Feng,

* Corresponding author.
E-mail address: squ@zju.edu.cn (S. Qu).

https://doi.org/10.1016/j.jmps.2018.01.002
0022-5096/

1970; Yang and Hsu, 1971). It acts as an essential technique to evaluate the mechanical properties of materials, especially for biomedical or small structures which are not feasible to produce a sample of well-defined dimensions (Aernouts et al., 2012; Ahearne et al., 2005; Yang et al., 2012; Zisis et al., 2015). However, the continuous indentation of the membrane by rigid objects could induce progressing large local deformation and even its ubiquitous puncture failure (Deris and Nadler, 2015; Nadler and Steigmann, 2006; Nguyen and Vu-Khanh, 2004; Nguyen et al., 2004; Steigmann, 2005). Knowing the puncture characteristics of the membrane by rigid objects can help avoid its failure in practical applications and make more reliable membrane structures.

The axisymmetric indentation of edge-supported soft elastomeric membranes by rigid objects with different profiles, such as flat-tipped, hemispherical-tipped and sharp-tipped cylindrical indenters has been studied extensively for different purposes (Liu et al., 2015; Pamplona et al., 2014; Pearce et al., 2011; Scott et al., 2004). The soft elastomeric membrane features large deformation and large strain when subjected to the loads applied in a transverse direction. Yang and Feng described the axisymmetric deformation of an elastomeric membrane by three first-order nonlinear ordinary differential equations and solved the problem of a circular flat membrane indented by a smooth sphere (Yang and Feng, 1970; Yang and Hsu, 1971). Begley et al. (2004) presented a closed-form solution for frictionless spherical indenter by approximating the contact and freestanding regions of the membrane separately. Adopting the Coulomb friction law to model the contact between the indenter and rubber membrane, and using the commercial finite-element code ABAQUS/Standard (2004), Selvadurai (2006) investigated the centric and eccentric indentation of a rigid spherical indenter on a rubber membrane. To model the phenomena of seed germination in nature, Pearce et al. (2011) studied the indentation of an initially curved membrane by a rigid body (Pearce et al., 2011).

Compared with the indentation of soft elastomeric membrane, puncture failure of soft elastomeric membrane is a more complicated topic with rare existing studies. During puncture failure, the soft elastomeric membrane experiences a rapid change from the intact configuration to the punctured configuration. The previous studies on puncture failure of soft elastomeric membranes usually were focused on the large local deformation around the indenter tip and the intrinsic material parameters controlling the puncture resistance of these materials (Deris and Nadler, 2015; Nadler and Steigmann, 2006; Steigmann, 2005). Dean et al. and Leslie et al. investigated the effects of the size and shape of the medical needle on the puncture failure of protective glove materials (Dean et al., 2008; Leslie et al., 1996). The experimental observations show that needle punctures gradually through the thickness of the elastomeric membrane, just as the needle cutting into the membrane. Nguyen et al. punctured different soft elastomer membranes with flat-tipped, rounded-tipped and conical-tipped cylindrical indenters. They concluded that the puncture failure of the membranes is not due to the stress concentration around the edge of the flat-tipped indenter, but controlled by an equi-biaxial deformation at the indenter tip that is independent of the indenter's diameter and geometry (Nguyen and Vu-Khanh, 2004; Nguyen et al., 2004). Furthermore, they developed a method to evaluate the fracture energy for puncture (Nguyen et al., 2009). In Nadler et al.'s work, an energy argument was used to predict the puncture failure of a membrane by a rigid indenter. Once the resultant strain energy of the deformed membrane exceeds the strain energy of the punctured membrane, the puncture failure of the membrane occurs (Nadler and Steigmann, 2006). Deris et al. used the global failure and maximum local deformation criteria to predict the puncture of the inflated elastomeric membrane by a rigid indenter (Deris and Nadler, 2015). It showed that local failure dominates the puncture for indenter with small radius, while global failure for indenter with large radius. Steigmann used membrane theory to analyze the puncture of a thin solid circular isotropic elastomeric sheet by a rigid axisymmetric indenter. In their analysis, the contact between the indenter and sheet is frictionless and once the total energy of the punctured state of the sheet is energetically favored over un-punctured state, the membrane is penetrated by the indenter (Steigmann, 2005).

Most of the previous studies on deformation and puncture failure of soft elastomeric membrane by rigid indenter assume the frictionless contact between the indenter and membrane. To our knowledge, there is no analytical model considering the effect of friction between the indenter and membrane in the study of the puncture failure. The frictionless assumption has the advantage of giving simple solution, but may not accurately capture the deformation details of the membrane around the indenter tip. Our experiment shows that the large local deformation around the indenter is significantly influenced by the friction, and so is the puncture failure. That means considering the friction between the membrane and indenter surface is necessary in studying the puncture failure. However, due to the very low elastomeric modulus and the high internal friction of rubber, the friction contact between rubber-like material and solid surface differs in many ways from the frictional properties of most other solids (Blau, 2001; Lorenz et al., 2011; Persson, 2001). Predicting the friction properties of rubber-like material is an intractable issue that is beyond the scope of this paper. The biggest challenge lies in the fact that the friction can be influenced by many factors in a wide spectrum of geometrical, physical and chemical situations (Persson, 2001). In fact, there is no universal and predictive theory for that. The phenomenological Coulomb friction model with a coefficient of friction is an alternative approach to evaluate the friction contact between the rigid and rubber-like materials. It is widely adopted in most practical applications, such as tire dynamics (Lorenz et al., 2011). Selvadurai (2006) used it to describe the friction contact between the brass plate and natural rubber. He observed the classic "slip-stick" phenomena at high rates of relative movement between the brass plate and rubber membrane, but found that the average coefficient of friction was almost independent of the rate of the relative movement. In this work, we also adopt Coulomb friction law to describe the friction contact between the soft elastomeric membrane and the indenter, with the coefficient of friction obtained by experiment.

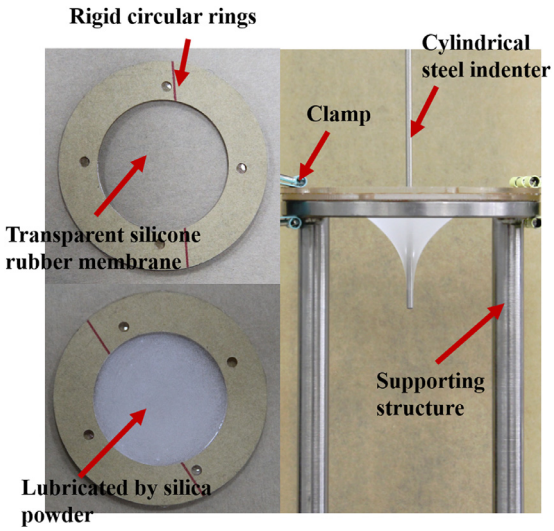

Fig. 1. The experiment setup: the silicone rubber membrane is initially flat and its boundary is constrained by rigid circular rings. Silica powder is used there to lubricate the surface of the membrane. The membrane is clamped on a supporting structure through rigid circular rings and then is indented and punctured by cylindrical steel indenter along its axial direction.

Fig. 2. The profile evolution of the membrane subjected to the continuous indentation by the cylindrical steel indenter with radius of 3 mm. The configuration of the highly deformed membrane consists of three parts. Part I is the region which doesn't contact with the indenter, Part II contacts with the indenter along its side surface, and Part III contacts with the indenter along its flat-tipped surface.

This work studies the large deformation and puncture failure of silicone rubber membrane by rigid cylindrical indenters experimentally and theoretically. We consider the effects of the indenter size and the membrane-indenter friction on the puncture failure of the membrane. The paper is organized as follows. Section 2 describes the experimental setup and observations. Section 3 presents the formulation of the analytical model. In Section 4, the results from the experiment and the analytical model are compared, and Section 5 lists the final conclusions.

2. Experiment

2.1. Puncture experiment of the silicone rubber membrane by rigid cylindrical indenters

As shown in Fig. 1, the setup of the puncture experiment includes the silicone rubber membrane with its boundary constrained by rigid circular rings (the inner and outer radius are constants of 25 mm and 40 mm respectively), the cylindrical steel indenters with different radius (1, 2, 3, and 4 mm), a supporting structure, and clamps used to fix the rigid rings on the supporting structure. To lubricate the contact between the membrane and indenter, the surface of the membrane is covered with a thin layer of silica powder. The silicone rubber membrane with thickness 0.2 mm used in our experiment is produced by the ZHONGYI CARBON TECHNOLOGY CO., LTD. Zhejiang, China. We conduct the puncture experiment using the uniaxial tensile testing machine. The cylindrical steel indenter is fixed with the mobile grip of the uniaxial tensile machine, and moves at a velocity of 5 mm/min to indent and penetrate the membrane along its axial direction. The shape evolution of the membrane under loading is shown in Fig. 2. As indicated, we divide the highly deformed membrane into three parts: non-contacting Part I, side-contacting Part II and flat end-contacting Part III.

In the experiment, we explore the effects of the indenter size and indenter-membrane friction on the membrane's puncture failure. The silicone rubber membranes with lubricated surface are punctured by the cylindrical steel indenters with different radius. The results are shown in Fig. 3(a). We find that the displacement–force curves don't show a monotonous relationship. The force increases synchronously at the beginning, then almost keeps constant and finally increases monotonously again with the increment of the displacement-controlled loading until the indenter penetrates the membrane and the corresponding reaction force on the indenter drops to almost zero. The larger the radius of the indenter, the longer the range of

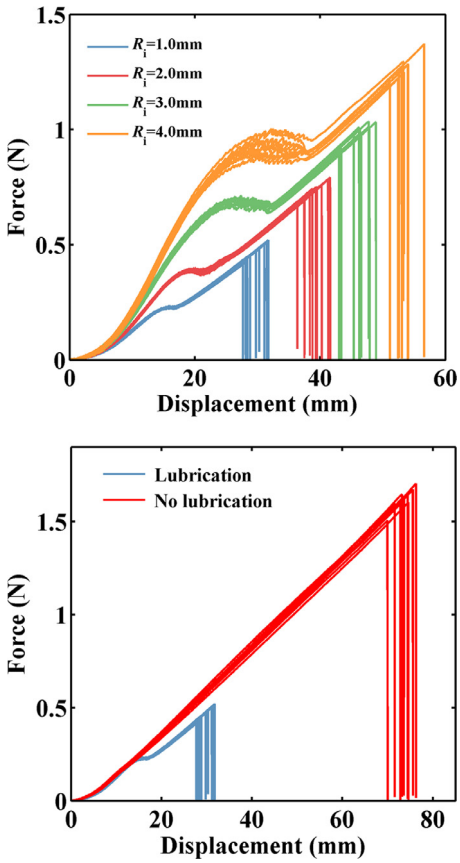

Fig. 3. (a) Experimental results of the displacement–force relationships (with displacement-controlled loading velocity of 5 mm/min) for silicone rubber membrane with lubricated surface. The indenters with radius of 1, 2, 3, and 4 mm are adopted in the experiment and ten membranes are punctured for each indenter. Once the indenter penetrates the membrane, the reaction force on the indenter drops drastically. (b) Comparison of the displacement–force relationships (with displacement-controlled loading velocity of 5 mm/min) for silicone rubber membranes with and without lubricated surface. The radius of the indenter is kept as1 mm.

the displacement in which the reaction force almost keeps as a constant. The results also indicate that indenter with smaller diameter needs less force to puncture the membrane. To show the importance of the friction between the indenter and the membrane, an indenter with radius 1.0 mm is used to puncture the membranes with and without surface lubrication. The displacement–force curves are shown in Fig. 3(b). The results clearly demonstrate the significance of the membrane-indenter friction in the puncture failure: the membrane not being lubricated resists the puncture failure more efficiently than the one with lubricated surface. We also observe different configurations of the membrane after being punctured. Membranes with lubricated surface are left with ohm-like curved cracks without losing mass (Fig. 4(a and b)). While the membranes without lubricated surfaces are penetrated through by the indenter and are left with circular-like holes after losing the central pieces (Fig. 4(c–e)).

2.2. The friction contact between the silicone rubber membrane and steel indenter

In the present study, we use Coulomb friction model to describe the friction contact between the membrane and indenter and determine the coefficient of friction experimentally. The silicone rubber membrane with initial thickness 0.2 mm and lubricated surface is fixed on a horizontal rigid plane sheet. A steel block of weight 0.3 N is pulled by a rope and slides on the surface of the membrane at a velocity of 5 mm/min. The material of the block and indenters are the same (304 stainless steel) and their surfaces undergo the same polishing processes to guarantee the same surface roughness. We repeat the experiment four times and Fig. 5(a) shows the relationship between the sliding displacement and the ratio of the pulling force to the weight of the steel block. The pulling force almost keeps as a constant once the block slides steadily on the membrane surface, so the coefficient of friction is taken as the ratio of the steady pulling force to the weight of the block. Because the value from the four experiments has slight fluctuation, we adopt the average of 0.18 as the friction coefficient in our work.

For the membrane without lubricated surface, its contact with the steel block seems so sticky that the relatively sliding between the two surfaces is difficult. Fig. 5b illustrates the pulling force divided by the weight (0.1 N) of the block versus

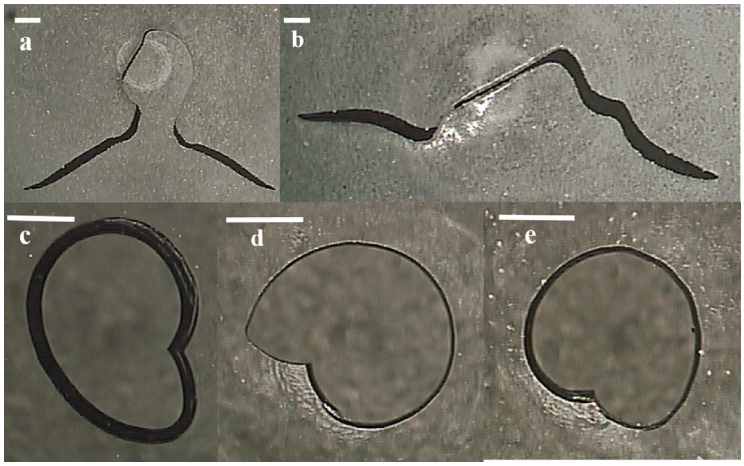

Fig. 4. Typical morphologies of the silicone rubber membranes after being punctured by the indenter. (a) and (b) are the membranes with lubricated surface punctured by the indenter with radius of 4 mm, while (c)–(e) are the membranes without lubricated surface punctured by the indenter with radius of 1 mm. The bar in pictures presents the length of 1 mm.

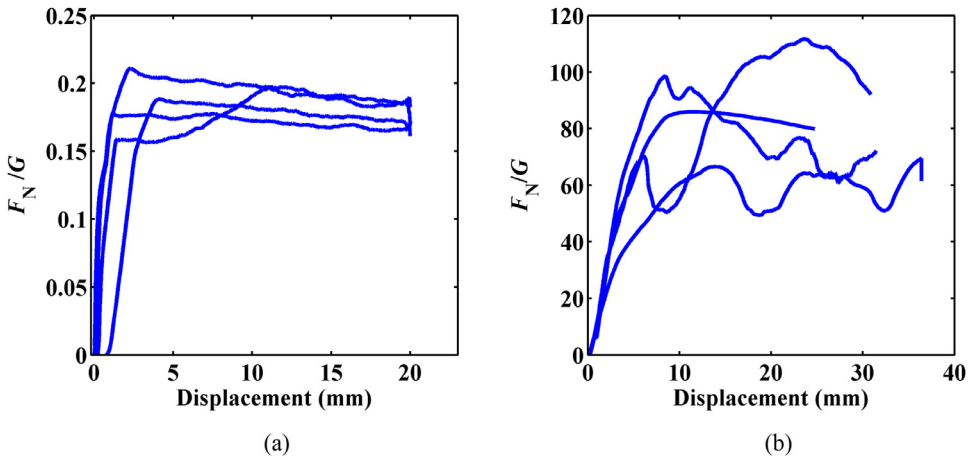

Fig. 5. The relationship between the sliding displacement (with displacement-controlled loading velocity of 5 mm/min) and traction force divided by the weight of the block. (a) The surface of the membrane is lubricated with silica powder and the weight of the steel block is 0.3 N. (b) The membrane isn't lubricated and the weight of the steel block is 0.1 N.

the controlled displacement. The peak force is almost up to 100 times of the weight of the steel block. The force on the rope mainly results from the shear deformation of the membrane while the block adheres on the membrane tightly and is difficult to slide. For this case of no lubrication, we can't obtain the coefficient of friction between the indenter and membrane by this way. Fortunately, based on the analytical model to be presented in the next section, we can obtain the coefficient by combining the model and the experimental data. This will be discussed in Section 4.

2.3. The critical stretch of the silicone rubber membrane

The fracture of rubber-like materials can be roughly classified into two scenarios. The first one studies the existing crack propagation in rubber-like materials since the pioneering work by Rivlin and Thomas (1953). Whereas the second one assumes that there are no cracks in the materials and the facture means the crack nucleation and propagation. The present puncture work belongs to the second one and the following discussion on the fracture criteria for rubber-like material is also related to this type. The existing fracture criteria for local failure mode can be divided into stress-based and stretch-based. However, based on their experimental findings, some researchers observed that the critical stress (such as the von Mises or Tresca stress) of the rubber-like material for fracture is related to the deformation state (Dickie and Smith, 1969; Smith and Rinde, 1969). For the stretch-based criteria, the commonly used ones are the maximum principal stretch criterion or the maximum equivalent stretch criterion. The maximum principal stretch criterion predicts that the material will fracture once the maximum principal stretch exceeds the critical one. But some existing experimental results also show that the maximum principal stretches of the rubber-like material are different for different deformation mode

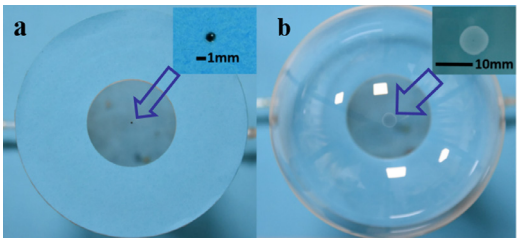

Fig. 6. (a) An initially flat silicone rubber membrane is constrained axisymmetrically and fixed on an air chamber. A circular mark with radius of 0.5 mm is made at the center of the membrane. (b) The membrane is inflated slowly and we record the radius of the mark to obtain the deformation at the center of the membrane.

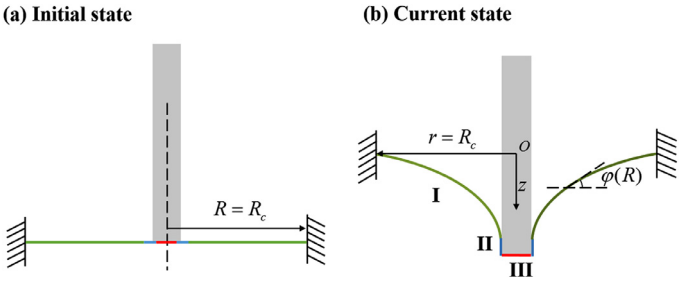

Fig. 7. Two states of the membrane in the analytical model. (a) The initial state. The membrane is initially flat and coordinate R is adopted to locate the material particle. (b) The current state. The configuration of the highly deformed membrane which is described using coordinates (r, z) consists of three Parts. φ is the tangential slope of the membrane with respect to the horizontal direction.

(Dickie and Smith, 1969; Hamdi et al., 2006; Hamdi et al., 2007). It seems that a reasonable criterion for predicting the local mode of failure for rubber-like material should take the deformation state into account and include all the three principal stretches in the formulation. Based on this idea, Hamdi et al., (2006, 2007) proposed a new failure criterion for rubber-like materials based on an equivalent elongation concept which includes the three principal stretches. This criterion has two fitting parameters and agrees well with ultimate extensibility of rubber-like materials under different deformation modes (such as uni-axial, equi-biaxial stretch and pure shear). Another simpler criterion describing the maximum extensibility of rubber under different types of deformation adopts the first invariant of right Cauchy-Green tensor $I_1 = {\lambda_1}^2 + {\lambda_2}^2 + {\lambda_3}^2$ (Gent, 2005). In this paper, Gent cited the experimental results from Dickie and Smith (1971) which shows the maximum extensibility of rubber in equi-biaxial stretching is only about 70% of that in simple extension.

In our study, we take the critical I_1, the first invariant of the right Cauchy–Green deformation tensor, as the maximum equivalent stretch of the hyperelastic membrane. In the previous literatures, the membrane inflation experiment is utilized to obtain the critical equi-biaxial stretch of the hyperelastic membrane (Dickie and Smith, 1969; Hamdi et al., 2006). Similarly, the critical value of I_1, as a material property, can be obtained through experiment directly by this way. As shown in Fig. 6, an initially flat silicone rubber membrane is constrained axisymmetrically and then inflated by pumping air slowly. The material of the membrane is the same as that used in the puncture experiment and the initial radius of the membrane is 30 mm. In the initial state, we mark a dot in the center of the membrane where the deformation is the largest. While inflating the membrane, we record the deformation of the mark continuously until the membrane explodes. The ratio of the radius of the mark when the membrane explodes divided by its initial radius gives two principal stretches at the critical state. The third one is obtained by incompressibility. Consequently, we obtain the critical value of the first invariant I_1, which is 95.2 ± 4.8 after we repeat the experiment four times. Strictly speaking, the critical stretch we obtain is from the average of a small area around the center, instead of a point. However, since the deformation around the center of the membrane is quite uniform and the initial diameter of the mark is about 1 mm, which is small enough compared with the diameter of the membrane, we assume the obtained value is close enough to the true critical value. And further, we assume the puncture failure of the membrane occurs at the same critical value of I_1.

3. Formulation

3.1. Indentation of the membrane by cylindrical indenter

In this section, the analytical model based on continuum mechanics is developed to study the large deformation and puncture failure of the membrane theoretically. The deformed membrane takes an out-of-plane axisymmetric configuration, as illustrated in Fig. 7. In the initial state, the membrane is flat and coordinate R is used to locate the material particle. While in the current state, coordinates (r, z) are adopted to describe the deformation of the membrane. The current configuration of the membrane consists of Parts I and III at the beginning of loading and then Part II of the membrane occurs with the

continuous indentation by the indenter. We define the stretches along the radial direction of the membrane as λ_1 and the circumferential direction as λ_2. The incompressibility of the material yields the stretch along the thickness direction as

$$\lambda_3 = \frac{1}{\lambda_1 \lambda_2}. \tag{1}$$

Therefore, the governing equations describing the current configuration of the membrane can be expressed by two variables, λ_1 and λ_2.

From the Helmholtz free energy density of the membrane $W(\lambda_1, \lambda_2)$, s_1 and s_2, the nominal stresses along the radial and circumferential directions can be obtained as (Ogden et al., 2004)

$$s_1 = \frac{\partial W(\lambda_1, \lambda_2)}{\partial \lambda_1} \tag{2}$$

$$s_2 = \frac{\partial W(\lambda_1, \lambda_2)}{\partial \lambda_2}. \tag{3}$$

Once the free energy density function $W(\lambda_1, \lambda_2)$ is determined, s_1 ands_2 can be calculated by Eqs. (2) and (3). In this study, we adopt Gent model as the material model which is suitable to describe the elasticity and the stiffening effect of polymer (Gent, 1995; Puglisi and Saccomandi, 2015). It is worth noting that there is a modified Gent model (the so called Gent–Gent model) with the form of $W = W(I_1, I_2)$, where I_1 and I_2 are the first and second invariants of the right Cauchy–Green deformation tensor (Pucci and Saccomandi, 2002; Ogden et al., 2004). For the Gent–Gent model, it has a pretty good theoretical prediction quantitatively on the uniaxial extension data for rubber in all range of uniaxial extension (Destrade et al., 2016). For the Gent model, it describes the mechanical behavior of rubber well in large deformation, but not so well for small and moderate extension. In our study on the puncture failure of the silicone rubber membrane, the stretch of the membrane near the indenter tip is definitely very large. And the left part of the membrane besides near the indenter is also relatively not so small considering the membrane is highly indented. Based on this, the Gent model with the form of $W = W(I_1)$ is acceptable in this study. Furthermore, the functional simplicity of Gent model makes it convenient to calculate the highly inhomogeneous stretch field of the membrane. In Gent model, the free energy density function is defined as

$$W = -\frac{\mu J_{\lim}}{2} \ln\left(1 - \frac{{\lambda_1}^2 + {\lambda_2}^2 + {\lambda_3}^2 - 3}{J_{\lim}}\right), \tag{4}$$

where μ is the shear modulus, and $J_{\lim}$ is a material constant defining the limit stretch. Substituting Eq. (4) into Eqs. (2) and (3), we obtain the following equations for the nominal stresses

$$s_1 = \frac{\mu({\lambda_1}^2 - {\lambda_3}^2)}{\lambda_1(1 - ({\lambda_1}^2 + {\lambda_2}^2 + {\lambda_3}^2 - 3)/J_{\lim})}, \tag{5}$$

$$s_2 = \frac{\mu({\lambda_2}^2 - {\lambda_3}^2)}{\lambda_2(1 - ({\lambda_1}^2 + {\lambda_2}^2 + {\lambda_3}^2 - 3)/J_{\lim})}. \tag{6}$$

Considering the current configuration of the Part I, as shown in Fig. 7, geometric relations require

$$\lambda_2 = \frac{r}{R}, \tag{7}$$

$$\frac{dr}{dR} = \lambda_1 \cos\varphi, \tag{8}$$

$$\frac{dz}{dR} = \lambda_1 \sin\varphi, \tag{9}$$

where φ is the tangential slope of the membrane with respect to the horizontal direction.

Differentiating Eq. (7) with respect to R gives

$$\frac{d\lambda_2}{dR} = \frac{dr}{RdR} - \frac{r}{R^2}. \tag{10}$$

Substituting Eq. (10) into Eq. (8) yields

$$\frac{d\lambda_2}{dR} = \frac{\lambda_1 \cos\varphi - \lambda_2}{R}. \tag{11}$$

For Part I of the membrane, it is not in contact with the indenter, so the surface is traction free. The force balance of the membrane along the z-direction (Fig. 8(a)) yields

$$2\pi s_1 R H_0 \sin\varphi = F, \tag{12}$$

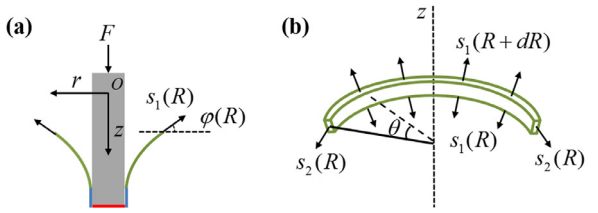

Fig. 8. (a) Material particle of the membrane to describe the mechanical equilibrium at Part I in the vertical direction. (b) Free-body diagram of half of the circular truncated cone at Part I to describe the mechanical equilibrium in the circumferential direction. $s_1(R)$ and $s_2(R)$ are the nominal stresses along the radial and circumferential directions of the membrane.

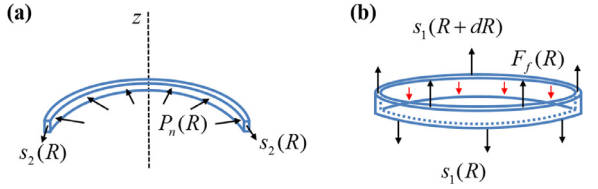

Fig. 9. Free-body diagrams of the membrane particle in the current state at Part II to describe the mechanical equilibrium. (a) Half of the axisymmetric deformed membrane particle. (b) The axisymmetric deformed membrane particle.$P_n(R)$ is the pressure between the indenter and the membrane and $s_2(R)$ is the nominal stress along the circumferential direction of the membrane. $s_1(R)$ is the nominal stress along the radial direction of the membrane and $F_f(R)$ is the friction force between the indenter and the membrane.

where F is the force applied on the indenter, and H_0 is the initial thickness of the membrane. Considering the force balance along the circumferential direction for half of the circular truncated cone (Fig. 8(b)) yields

$$\frac{d}{dR}(Rs_1\cos\varphi) = s_2 \tag{13}$$

Eqs. (9), (11), (12), and (13) construct the governing equations describing the current configuration of Part I.

For Part II of the membrane, which is in contact with the indenter along the side surface, the geometric relations require

$$\lambda_1 = \frac{dz}{dR}, \tag{14}$$

$$\lambda_2 = \frac{R_i}{R}, \tag{15}$$

where R_i is the radius of the indenter.

The true pressure P_n between the indenter and the membrane can be obtained by considering the force balance of the material particle (shown in Fig. 9(a)) of Part II as

$$P_n = \frac{s_2 H_0}{\lambda_1 R_i}. \tag{16}$$

Force balance in the z-direction of the membrane, as shown in Fig. 9(b), yields

$$\frac{ds_1}{dR} = \frac{\lambda_1\lambda_2}{H_0}\mu' P_n, \tag{17}$$

where μ' is the coefficient of friction in the Coulomb friction model and $\mu' P_n$ is the true shear traction due to the friction. Substituting Eq. (16) into Eq. (17) gives

$$\frac{ds_1}{dR} = \frac{1}{R_i}\mu'\lambda_2 s_2. \tag{18}$$

Eqs. (14), (15), and (18) are the governing equations for Part II of the membrane. The Part III membrane at the flat-tipped indenter undergoes uniform deformation which can be obtained by the continuous conditions between the Part II and III.

The continuity conditions between Part I and Part II of the membrane are

$$\begin{aligned} \lambda_1{}^{I} &= \lambda_1{}^{II} \\ \lambda_2{}^{I} &= \lambda_2{}^{II}. \end{aligned} \tag{19}$$

The superscripts I and II denote Part I and Part II of the membrane. One of two continuity conditions between Part II and Part III is

$$\lambda_2{}^{II} = \lambda_2{}^{III}. \tag{20}$$

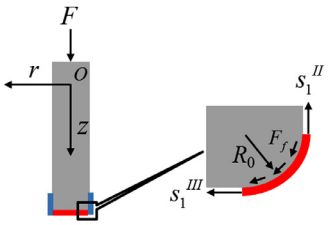

Fig. 10. The stress state of the membrane at the corner of the indenter. $s_1{}^{II}$ is the nominal stress along radial direction at Part II of the membrane. $s_1{}^{III}$ is the nominal stress along radial direction at Part III of the membrane. F_f is the friction force between the indenter and the membrane.

The other continuity condition is related to the friction between the indenter and membrane. $s_1{}^{II}$and $s_1{}^{III}$ are the nominal stresses along the radial direction of the membrane at the two sides of the corner of the indenter, as shown in Fig. 10. $s_1{}^{III}$ is the stress at Part III and $s_1{}^{II}$ at the bottom of Part II. We take the corner of the cylindrical indenter as a smooth circular arc with a small radius R_0 which is in accordance with the indenter used in the experiment. As shown in Fig. 10, the stress along the radial direction of the membrane and the friction between the membrane and indenter satisfy

$$\frac{ds_1}{dc} = \frac{\mu'}{R_c} s_1, \tag{21}$$

where c is the arc length of the membrane around the indenter corner, and R_0 is the radius of the arc as shown in Fig. 10. Strictly speaking, the friction on the membrane at the corner has contributions from the two principle curvatures of the indenter. Besides the one shown in Fig. 10, the other one is the curvature of the side surface of the indenter. However, the latter one is much smaller than the previous one and is neglected when obtaining Eq. (21). Integrating Eq. (21) along the corner from Part III to Part II of the membrane, we obtain the following additional continuity condition between Part III and Part II as

$$\frac{s_1{}^{II}}{s_1{}^{III}} = \exp(\mu'\pi/2). \tag{22}$$

Eqs. (20) and (22) consist of the continuity conditions between Part II and Part III of the membrane. Moreover, before the occurrence of Part II at the beginning of loading, the continuity conditions between Part I and Part III are

$$\begin{aligned} &\lambda_2{}^{I} = \lambda_2{}^{III} \\ &\frac{s_1{}^{III}}{s_1{}^{I}} = \exp(\mu'\varphi) \end{aligned}, \tag{23}$$

where φ is the tangential slope of the membrane at the bottom of Part I with respect to the horizontal direction. The membrane is constrained by the rigid ring and has no prestretch, consequently,

$$\lambda_2(R_c) = 1, \tag{24}$$

where R_c is the inner radius of the rigid rings.

By integrating the puncture criterion of critical stretch into the analytical model, we can predict the puncture failure of the membrane. In the analytical model, we assume the puncture failure occurs when the maximum value of I_1, the first invariant of right Cauchy–Green deformation tensor, reaches the critical value.

3.2. Two stages of the displacement-controlled loading

Based on the experimental displacement-controlled loading curves, the loading procedure of the membrane with lubricated surface is divided into two stages. At the beginning of loading, the stresses in the membrane are not large enough to overcome the resistance force to sliding from the corner of the indenter, so the deformation of Part III is constrained. The boundary of Part III is constrained and we take the stage as a fixed boundary condition one. Once the stress in the membrane is large enough due to the continuous indentation by the indenter to overcome the resistance force to sliding, Part III begins to slide outside along the surface of the indenter. The sliding of the membrane could release the stress around the indenter tip and the corresponding reaction force on the indenter in turn, restricting the further sliding of the membrane. On the other hand, the continuous indentation of the indenter will increase the stress around the indenter tip and drive the membrane to slide further again. That's why we can observe the "stick-slip" phenomenon and the almost invariant force in the middle of force–displacement curve from the displacement-controlled experiment, as shown in Fig. 3a. Once the membrane begins to slide along the surface of the indenter, the boundary of the Part III varies and the stage is taken as a slip boundary condition one. For the membrane without lubricated surface, the membrane and the surface of the indenter stick together so tight that the membrane can hardly slide on the surface of the indenter. This is the reason why the displacement–force curves just show a monotonically increasing relationship.

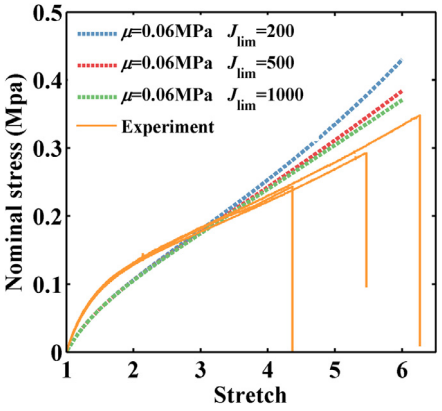

Fig. 11. Fitting the uniaxial stretch experiment results with Gent model.

3.3. Method of solving the differential equations

Given the boundary conditions, we use shooting method to solve the above ordinary differential equations. At the stage that the deformation of the membrane at Part III is constrained, the problem is simplified as a fixed boundary condition one. The initial value of the stretch along the radial direction of the membrane λ_1 at the inner boundary of Part I is adjusted until the solution satisfies the boundary condition at $R = R_0$. As discussed above, when the stress in the membrane around the indenter tip is large enough to overcome the resistance force from the corner of the indenter, the membrane at Part III begins to slide along the surface of the indenter and the problem becomes a slip boundary condition one. For this stage, two different scenarios, with and without Part II, are discussed separately. Before the occurrence of Part II, the initial values of the stretches along the radial and circumferential directions λ_1 and λ_2 at the inner boundary of Part I are adjusted until the solution satisfies the outer boundary condition at $R = R_c$. And the stretch at Part III of the membrane can be obtained using the continuity conditions between the two Parts. If Part II exists, the initial value λ_2 at the inner boundary ($R = R_i/\lambda_2$, where R_i is the radius of the indenter) of Part I is adjusted until the solution satisfies the boundary condition $\lambda_2(R_c) = 1$at $R = R_c$. The outer boundary of Part II, same as the inner boundary of Part I, can be determined. Using the continuity conditions between Parts I and II, the deformation field of Part II is calculated as an initial-value problem. Noting that initially we don't know the inner boundary of Part II, we just keep the calculation going forward to the center of the membrane until the newly calculated stretch (${\lambda_1}^{II}$, ${\lambda_2}^{II}$) satisfies one of the continuum condition $\frac{{s_1}^{II}}{{s_1}^{III}} = \exp(\mu'\pi/2)$ between Parts II and III, where ${s_1}^{II}$and ${s_1}^{III}$ are the radial stresses at the two sides of the intersection between Parts II and III, and μ' is the coefficient of friction between the membrane and indenter. The inner boundary of Part II, also the outer boundary of Part III, can be determined as $R = R_i/{\lambda_2}^{II}$. The radial stress at the inner boundary of Part II is ${s_1}^{II} = {s_1}^{II}({\lambda_1}^{II}, {\lambda_2}^{II})$. Considering the other continuum condition between Parts II and III ${\lambda_2}^{III} = {\lambda_2}^{II}$, the homogeneous deformation at Part III results in the stress ${s_1}^{III} = {s_1}^{III}({\lambda_2}^{III})$. Moreover, the length of Part II is calculated as the difference between its two boundaries, i.e., the inner one and the outer one.

4. Results and discussions

4.1. Material parameters of the silicone rubber membrane

In this section, the experimental and analytical results are presented. The deformed membrane undergoes inhomogeneous biaxial deformation, leading to anisotropic mechanical response. However, except that around the tip of the indenter, the stretch along the circumferential direction of the membrane is nearly negligible compared with the large radial stretch of the membrane. We obtain the material parameters by fitting the experimental uniaxial stretch stress relationship of the silicone rubber membrane. Three specimens (width 10 mm, thickness 0.2 mm, and length 60 mm) are stretched along the length direction at a velocity of 5 mm/min, the same as that adopted in the puncture experiments. The analytical and experimental results are shown in Fig. 11. We obtain the shear modulus of 0.06 Mpa after fitting the experimental data. However, as shown in the figure, the specimens fail before obvious stress strengthening occurs, and the force–displacement relation from the Gent model is insensitive to the limiting stretch $J_{\lim}$ before the final strengthening stage, consequently, the limit stretch $J_{\lim}$ in Gent model cannot be directly fitted from the above tensile experiment. We obtain $J_{\lim}$ by matching the critical stretch in the previous pneumatic experiment and the puncture test. An indenter of radius 2 mm is used to puncture the membrane. Use the force at the puncture failure as the input, we adjust the limiting stretch $J_{\lim}$ in Gent model until the calculated maximum stretch in the membrane equals to the critical value measured from the experiment. Finally, we obtain limiting stretch in Gent model, $J_{\lim} = 125$.

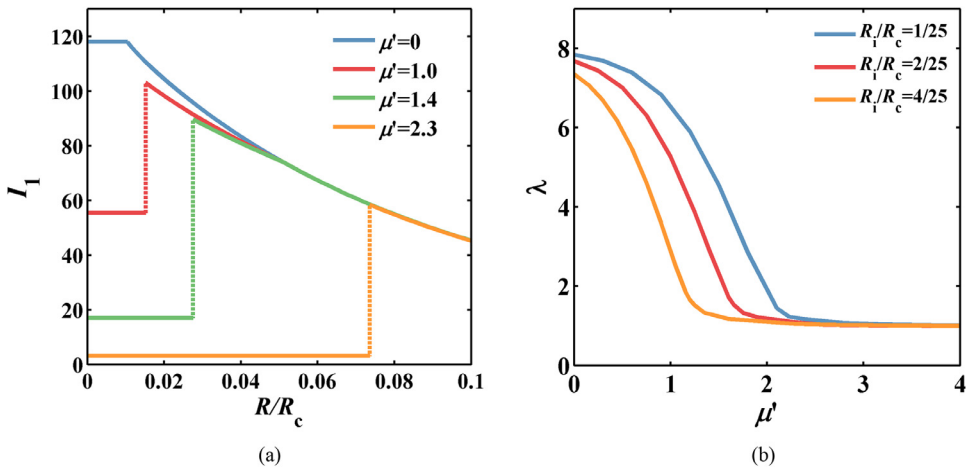

Fig. 12. (a) The first invariant of the right Cauchy–Green deformation tensor I_1 of the membrane along the radial direction (only the stretch around the indenter tip is illustrated to highlight the detail). The normalized radius R_i/R_0 of the indenter and the reaction force $F/2\pi H_0 R_0$ on the indenter are constant of 0.08 and 1 respectively. (b) The stretch of the membrane at the tip of the indenters with different radius. The normalized reaction force $F/2\pi H_0 R_0$ on the indenter is kept as constant 1. H_0 and R_0 are the initial thickness and the radius of the membrane.

4.2. The effect of friction contact on the deformation field of the membrane

Using the analytical model, this section explores the effect of friction between the indenter and membrane on the deformation field of the membrane near the indenter, by adjusting the coefficient of friction. The normalized force on the indenter $F/2\pi\mu H_0 R_0$ is kept as constant 1 in all the calculations. Fig. 12(a) shows the first invariant of the right Cauchy-Green deformation tensor I_1 along the radius direction. Only the stretch on and around the indenter tip is illustrated to show the difference. The far field deformation of the membrane is not affected by the localized friction at the tip and is almost same under the same force. In these calculations, the normalized radius of the indenter R_i/R_c is kept as 0.08. The drop of the lines in Fig. 12(a) results from the large friction at the corner of the indenter (Eq. 22). The ratio of the indenter radius to the location of the drop gives the stretching ratio in Part III. Fig. 12(b) shows the homogeneous stretch of the membrane at the tips of the three indenters (Part III of the membrane) of different radius. The results illustrate that friction has significant effect on the local deformation field of the membrane on and around the indenter tip. For small friction between the membrane and indenter, the membrane under the tip of the indenter undergoes a large biaxial stretch. When the friction coefficient is larger, the membrane on the indenter is more difficult to slide and is more constrained, so the maximum stretching is smaller. This explains why the larger the friction between the indenter and membrane, the larger the force needed to penetrate the membrane. The location of the maximum equivalent stretch of the membrane, where the crack initiates, is always at the corner of the indenter.

As shown in Fig. 4, the shapes of the membranes after being punctured are different for membranes with and without lubricated surfaces. This difference results from the distinct stretch fields of the membrane at the indenter tip. When puncture failure occurs, the elastomeric membrane experiences a rapid change from the intact configuration to the punctured configuration and the puncture process can be regarded as two stages (Fakhouri et al., 2015). At the first stage, the crack nucleates in the membrane at the corner of the indenter due to the large local deformation induced by the indenter. And then, the crack propagates through the fracture process zone until the indenter penetrates the membrane at the second stage. The fracture process zone is the region around the crack with large deformation (Persson et al., 2013). To drive the initial crack to grow in the membrane, two conditions must be met (Fakhouri et al., 2015). One is the stress in the membrane should be large enough to break the chemical bonds, and the other is the work provided by the fracture process zone should be sufficient to separate the newly created crack faces. For the case that the membrane is not lubricated, the constrained deformation at Part III is small. The highly deformed membrane is in the Part II and its neighbouring region of Part I. The crack initiates from Part of the corner of the indenter due to large deformation, but may not satisfy the energy requirement for propagating in opening mode, until the whole indenter penetrates the membrane. Therefore, for this case, the indenter eventually penetrates out a circular-like hole, which means the crack at the corner before the formation of hole doesn't propagate into the neighboring membrane. Due to the homogeneous deformation of the membrane at the tip of the indenter, the ratio of the diameter of the indenter over that of the circular-like hole gives the stretch of the membrane in Part III, which is 1.58 $\pm$ 0.14. Then in the analytical model, we apply the same puncture force as in the experiment and adjust the coefficient of friction until the calculated stretch in Part III matches the above value from the experiment. By this way, we obtain the coefficient of friction as 1.95 between the indenter and membrane without lubrication surface in the puncture experiment.

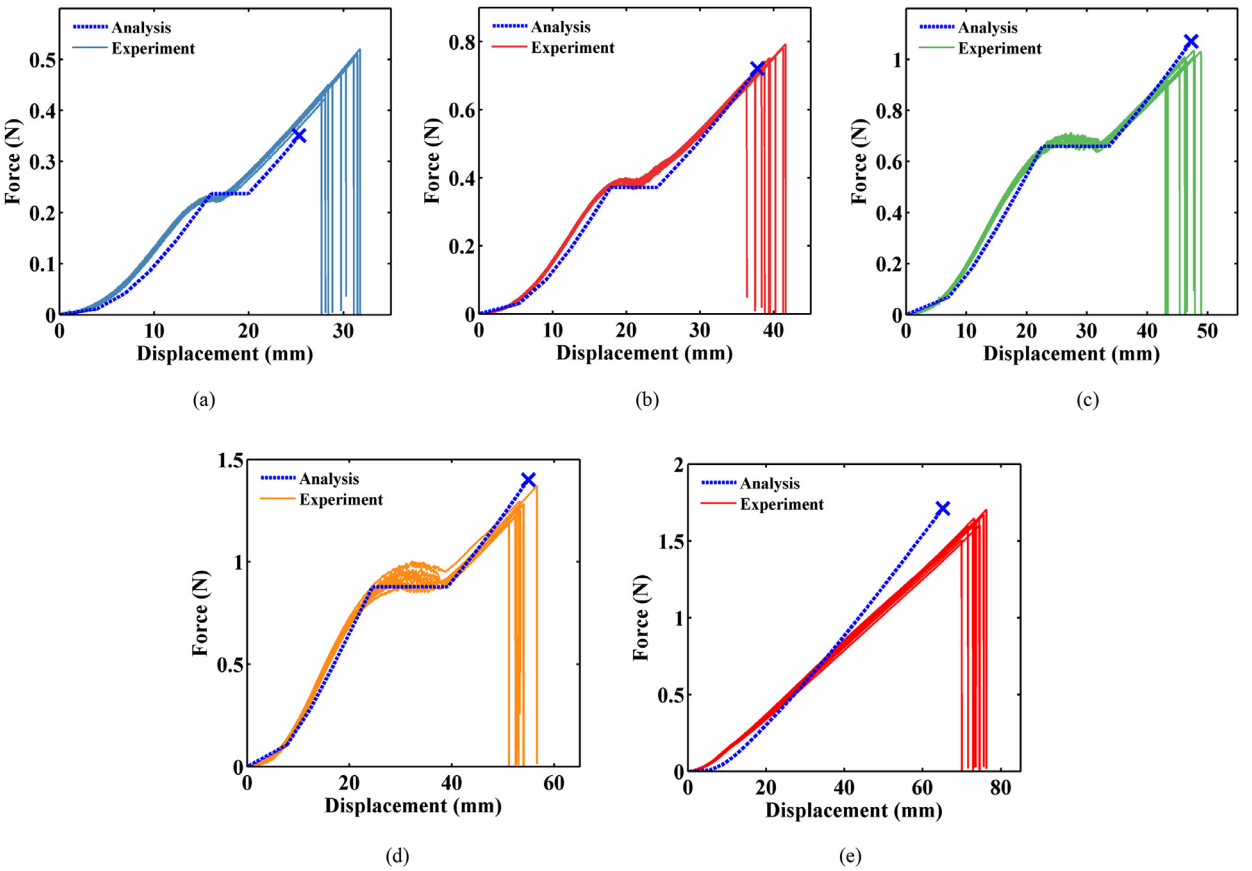

Fig. 13. Comparison between the analytical and experimental results. (a)–(d) show the displacement–force relationships of the membrane with lubricated surface indented and punctured by the indenter with radius of 1, 2, 3, and 4 mm. (e) shows the displacement–force relationships of the membrane without lubricated surface indented and punctured by the indenter with radius of 1 mm. The cross in the analytical results indicates the puncture failure of the membrane predicted by the analytical model. The dramatic drop of the force in the experimental results indicates the membranes being punctured by the indenter.

For the membrane with lubricated surface, deformation in Part III, II and near the indenter tip of Part I is concentrated. The crack initiates firstly from part of the corner of the indenter due to large deformation, and further grows around the corner by crack propagating. This occurs because the deformation is so large and so concentrated and the elastic energy stored is enough to drive the crack propagation. Because of the deformation localization in the membrane being lubricated, it is more flaw-sensitive in resisting puncture than the membrane without being lubricated.

4.3. Comparison between the analytical and experimental results

Adopt the initial shear modulus, limiting stretch J_{lim}, and coefficient of friction obtained in the previous two parts, we use the analytical model to predict the displacement–force curves for four indenters with radius 1 mm, 2 mm, 3 mm and 4 mm, respectively. The comparison with the experimental results is shown in Fig. 13(a)–(d). As discussed above, when the load is small, the membrane does not slide along the indenter and has no Part II contacting zone. The governing equations for Part I have fixed boundary conditions. When the stress in the membrane is large enough to overcome the resistance force from the corner of the indenter, the membrane at Part III begins to slide along the surface of the indenter. The plateau in the middle of the force–displacement curves in Fig. 13(a)–(d) should correspond to the initiation of the sliding and the formation of Part II zone. The cross mark in these figures indicate the maximum force predicted by the analytical model when the first invariant of the right Cauchy–Green deformation tensor I_1 reaches the critical value for membrane puncture. Fig. 13(e) is the same comparison for the membrane without being lubricated. Due to the large resistance force, the sliding on the surface of the indenter is small, so the corresponding stress relaxation is not sufficient to induce a plateau in the force displacement curves. The comparison of the analytical and experimental results in Fig. 13 shows that the analytical model does give a good prediction both on the displacement–force relationships and the puncture failure of the membrane.

As an example to illustrate the influence of friction contact on the puncture failure of elastomeric membrane, two inflated balloons are punctured using the cylindrical steel indenter with radius of 1 mm. The surface of one balloon is lubricated

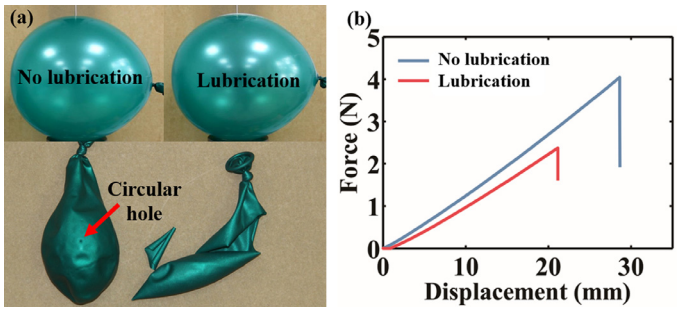

Fig. 14. (a) Two inflated balloons with the same air pressure are punctured by the cylindrical steel indenter with radius of 1 mm. One of the balloons is lubricated with silica powder while the other is not. The balloon with lubricated surface explodes at a critical load and is torn into two pieces. The balloon without lubricated surface is punctured along a circular-like ring which does not propagate again and the air runs slowly off the balloon. (b) The displacement–force relationships. The drop of the force indicates the puncture failure of the balloon.

with silica powder and the other is not lubricated. The initial inflation pressure of the two balloons is kept the same. The displacement–loading curves and the punctured states of the two balloons are shown in Fig. 14. As we can see, the balloon with lubricated surface is easier to be punctured by the indenter. The morphologies of the two balloons at punctured states are also different. The balloon with lubricated surface explodes at the critical load and is torn into two pieces. While the balloon without lubricated surface is punctured through along the edge of the indenter and the air leaks out of the balloon, a typical leak-before-break scenario. This demonstrates that for elastomeric membrane, sticky friction contact with the rigid indenter can resist the puncture failure more effectively. In our work, the diameter of the indenters is sufficiently large compared with the thickness of the membrane. It should be pointed out that singularity at the tip of the indenter can be induced if a membrane is indented and punctured by a sharp-tipped indenter, which is not suitable for the analytical model developed in this work.

5. Conclusions

Experiment and analysis have been conducted in order to investigate the large deformation and puncture failure of silicone rubber membrane by cylindrical steel indenters. We focus on the effects of friction contact between the membrane and indenter, as well as indenter size, on the deformation and puncture failure of the membrane. In the analytical model, the membrane is divided into three parts and the friction between the membrane and indenter is described by Coulomb friction model. The first invariant of the right Cauchy–Green deformation tensor I_1 of the membrane is adopted to predict the failure of the membrane. Once it reaches a critical value, the membrane is punctured. We find that the friction contact has significant influence on the local deformation of the membrane around the indenter tip and the puncture failure of the membrane. The experimental and analytical results show that the larger the friction coefficient between the indenter and membrane, the larger the force needed to puncture the membrane. The morphology of the membrane after being punctured by the indenter is also related to the friction condition with the indenter. Under the condition of large friction contact, a circular hole is left after the membrane being punctured. While for the membrane with lubricated surface, ohm-shaped line crack is observed.

Acknowledgments

This work is supported by the National Natural Science Foundation of China (Nos. 11525210, 11621062, 91748209), Zhejiang Provincial Natural Science Foundation of China(LZ14A020001), and the Fundamental Research Funds for the Central Universities.

Supplementary materials

Supplementary material associated with this article can be found, in the online version, at doi:10.1016/j.jmps.2018.01.002.

References

AernAernouts, J., Aerts, J.R.M., Dirckx, J.J.J., 2012. Mechanical properties of human tympanic membrane in the quasi-static regime from in situ point indentation measurements. Hearing Res 290, 45–54.
Ahearne, M., Yang, Y., El Haj, A.J., Then, K.Y., Liu, K.K., 2005. Characterizing the viscoelastic properties of thin hydrogel-based constructs for tissue engineering applications. J. R. Soc. Interface 2, 455–463.
Begley, M.R., Mackin, T.J., Begley, M.R., Mackin, T.J., 2004. Spherical indentation of freestanding circular thin films in the membrane regime. J. Mech. Phys. Solids 52, 2005–2023.
Blau, P.J., 2001. The significance and use of the friction coefficient. Tribol. Int. 34, 585–591.
Dean, S.W., Dolez, P.I., Vu-Khanh, T., Nguyen, C.T., Guero, G., Gauvin, C., Lara, J., Dean, S.W., Dolez, P.I., Vu-Khanh, T., 2008. Influence of medical needle characteristics on the resistance to puncture of protective glove materials. J. ASTM Int. 5, 101364–101375.

Deris, A.H.A., Nadler, B., 2015. Modeling the indentation and puncturing of inflated elastic membranes by rigid indenters. Int. J. Non-Linear Mech. 69, 29–36.
Destrade, M., Saccomandi, G., Sgura, I., 2016. Methodical fitting for mathematical models of rubber-like materials. Proc. R. Soc. A 473, 2198.
Dickie, R.A., Smith, T.L., 1969. Ultimate tensile properties of elastomers. VI. Strength and extensibility of a styrene-butadiene rubber vulcanizate in equal biaxial tension. J. Polym. Sci. A-2 Polym. Phys. 7, 687–707.
Dickie, R.A., Smith, T.L., 1971. Viscoelatic properties of a rubber vulcanizate under large deformation in equal biaxial tension, pure shear, and simple tension. Trans. Soc. Rheol. 15, 91–110.
Fakhouri, S., Hutchens, S.B., Crosby, A.J., 2015. Puncture mechanics of soft solids. Soft Matter 11, 4723–4730.
Gent, A.N., 1995. A new constitutive relation for rubber. Rubber Chem. Technol. 69, 59–61.
Gent, A.N., 2005. Extensibility of rubber under different types of deformation. J. Rheol. 49, 271–275.
Hamdi, A., Abdelaziz, M.N., Hocine, N.A., Heuillet, P., Benseddiq, N., 2006. A fracture criterion of rubber-like materials under plane stress conditions. Polym. Testing 25, 994–1005.
Hamdi, A., Abdelaziz, M.N., Hocine, N.A., Heuillet, P., Benseddiq, N., 2007. A new generalized fracture criterion of elastomers under quasi-static plane stress loadings. Polym. Testing 26, 896–902.
Leslie, L.F., Woods, J.A., Thacker, J.G., Morgan, R.F., Mcgregor, W., Edlich, R.F., 1996. Needle puncture resistance of surgical gloves, finger guards, and glove liners. J. Biomed. Mater. Res. 33, 41–46.
Liu, J., Mao, G., Huang, X., Zou, Z., Qu, S., 2015. Enhanced compressive sensing of dielectric elastomer sensor using a novel structure. J. Appl. Mech. 82, 101004.
Lorenz, B., Persson, B.N.J., Dieluweit, S., Tada, T., 2011. Rubber friction: Comparison of theory with experiment. Eur. Phys. J. E 34, 1–11.
Mao, G., Huang, X., Liu, J., Li, T., Qu, S., Yang, W., 2015. Dielectric elastomer peristaltic pump module with finite deformation. Smart Mater. Struct. 24, 075026.
Martinez, R.V., Branch, J.L., Fish, C.R., Jin, L., Shepherd, R.F., Nunes, R.M., Suo, Z., Whitesides, G.M., 2013. Robotic tentacles with three-dimensional mobility based on flexible elastomers. Adv. Mater. 25, 205–212.
Nadler, B., Steigmann, D.J., 2006. Modeling the indentation, penetration and cavitation of elastic membranes. J. Mech. Phys. Solids. 54, 2005–2029.
Nguyen, C.T., Vu-Khanh, T., 2004. Mechanics and mechanisms of puncture of elastomer membranes. J. Mater. Sci. Lett. 39, 7361–7364.
Nguyen, C.T., Vu-Khanh, T., Dolez, P.I., Lara, J., 2009. Puncture of elastomer membranes by medical needles. Part II: Mech. Int. J. Fract. 155, 83–91.
Nguyen, C.T., Vu-Khanh, T., Lara, J., Nguyen, C.T., Vu-Khanh, T., 2004. Puncture characterization of rubber membranes. Theor. Appl. Fract. Mech. 42, 25–33.
Ogden, R.W., Saccomandi, G., Sgura, I., 2004. Fitting hyperelastic models to experimental data. Comput. Mech. 34, 484–502.
Pamplona, D.C., Weber, H.I., Sampaio, G.R., 2014. Analytical, numerical and experimental analysis of continuous indentation of a flat hyperelastic circular membrane by a rigid cylindrical indenter. Int. J. Mech. Sci. 87, 18–25.
Parthasarathy, R., Groves, J.T., 2006. Curvature and spatial organization in biological membranes. Soft Matter 3, 24–33.
Pearce, S.P., King, J.R., Holdsworth, M.J., 2011. Axisymmetric indentation of curved elastic membranes by a convex rigid indenter. Int. J. Non-Linear Mech. 46, 1128–1138.
Persson, B.N.J., 2001. Theory of rubber friction and contact mechanics. J. Chem. Phys. 115, 3840–3861.
Persson, B.N.J., Albohr, O., Heinrich, G., Ueba, H., 2013. Crack propagation in rubber-like materials. J. Phys. Condens. Matter 17, 1071–1142.
Pucci, E., Saccomandi, G., 2002. A note on the Gent model for rubber-like materials. Rubber Chem. Technol. 75, 839–852.
Puglisi, G., Saccomandi, G., 2015. The Gent model for rubber-like materials: An appraisal for an ingenious and simple idea. Int. J. Non-Linear Mech. 68, 17–24.
Rivlin, R.S., Thomas, A.G., 1953. Rupture of rubber. I. Characteristic energy for tearing. J. Polym. Sci. 10, 291–318.
Scott, O.N., Begley, M.R., Komaragiri, U., Mackin, T.J., 2004. Indentation of freestanding circular elastomer films using spherical indenters. Acta Mater 52, 4877–4885.
Selvadurai, A.P.S., 2006. Deflections of a rubber membrane. J. Mech. Phys. Solids 54, 1093–1119.
Selvadurai, A.P.S., Yu, Q., 2006. On the indentation of a polymeric membrane. Proc. R. Soc. A 462, 189–209.
Smith, T.L., Rinde, J.A., 1969. Ultimate tensile properties of elastomer. V. Rupture in constrained biaxial tensions. J. Polym. Sci. A-2 Polym. Phys. 7, 675–685.
Steigmann, D., 2005. Puncturing a thin elastic sheet. Int. J. Non-Linear Mech. 40, 255–270.
Yang, W., Feng, W., 1970. On axisymmetrical deformations of nonlinear membranes. J. Appl. Mech. 37, 1002–1011.
Yang, W.H., Hsu, K.H., 1971. Indentation of a circular membrane. J. Appl. Mech. 38, 227–230.
Yang, Y., Liao, J., Lin, C.K., Chang, C., Wang, S., Ju, M., 2012. Characterization of cholesterol-depleted or -restored cell membranes by depth-sensing nano-indentation. Soft Matter 8, 682–687.
Zisis, T., Zafiropoulou, V.I., Giannakopoulos, A.E., 2015. Evaluation of material properties of incompressible hyperelastic materials based on instrumented indentation of an equal-biaxial prestretched substrate. Int. J. Solids Struct. 64-65, 132–144.